

Quinone-Modified Mn-Doped ZnS Quantum Dots for Room-Temperature Phosphorescence Sensing of Human Cancer Cells That Overexpress NQO1

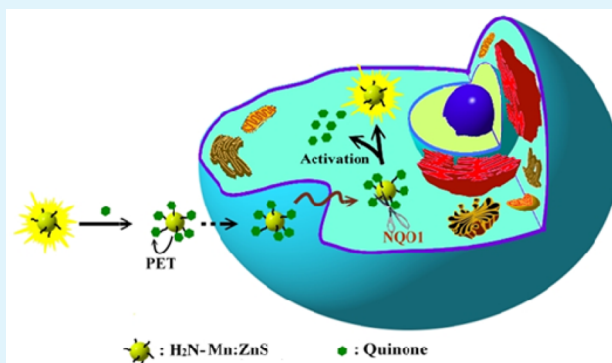
Yi-Ming Sung,[†] Srivardhan Reddy Gayam,[†] Pei-Ying Hsieh,[‡] Hsin-Yun Hsu,[†] Eric Wei-Guang Diao,[†] and Shu-Pao Wu^{*†}

[†]Department of Applied Chemistry and [‡]Center for Interdisciplinary Science (CIS), National Chiao Tung University, Hsinchu 300, Taiwan

S Supporting Information

ABSTRACT: Early detection of cancer cells in a rapid and sensitive approach is one of the great challenges in modern clinical cancer care. This study has demonstrated the first example of a rapid, selective, and sensitive phosphorescence probe based on phosphorescence energy transfer (PET) for cancer-associated human NAD(P)H:quinone oxidoreductase isozyme 1 (NQO1). An efficient room-temperature phosphorescence NQO1 probe was constructed by using Mn-doped ZnS quantum dots (Mn:ZnS QDs) as donors and trimethylquinone propionic acids as acceptors. Phosphorescence quenching of Mn:ZnS QDs from the Mn:ZnS QDs to a covalently bonded quinone was achieved through PET. Phosphorescence of Mn:ZnS QDs was turned on by the rapid reduction-initiated removal of the quinone quencher by NQO1. This probe shows low cellular toxicity and can rapidly distinguish between NQO1-expressing and -nonexpressing cancer cell lines through phosphorescence imaging.

KEYWORDS: room temperature phosphorescence, quantum dots, NQO1, cancer cells, phosphorescence energy transfer



INTRODUCTION

The development of rapid, highly sensitive, and selective probes for cancer-associated targets has been an important research topic because of their widespread applications in clinical diagnosis and treatments for cancer. Conventionally, extracellular or cell surface proteins are used as targets in recognizing cancer cells, resulting in poor selectivity and sensitivity of probes. Recently, the development of probes has focused on targeting endogenous cancer-associated enzymes.^{1–4} This approach helps to distinguish healthy tissue from diseased tissue and provides real-time information on cancer cells.

NQO1 (NAD(P)H:quinone oxidoreductase isozyme 1)^{5–7} is highly upregulated in cancer cells and is present in several human tumor cells such as those of the breast, colon, head and neck, kidney, lung, liver, ovaries, pancreas, and stomach at levels approximately 50-fold higher than those in normal tissue.^{8,9} The activity of NQO1 is strongly influenced by the life cycle of cancer cells. In particular, NQO1 is an antioxidant enzyme that catalyzes the two-electron reduction of quinones to their corresponding hydroquinones by using NADH as an electron donor.¹⁰ This reduction function of NQO1 has made it a suitable target for the design of prodrug therapies^{11–16} and profluorophores^{4,17} in cancer treatment and for the imaging of cancer cells.

Room-temperature phosphorescence (RTP) has been identified as a useful optical method that provides several advantages over the fluorescence method.¹⁸ Phosphorescence can be defined as radiative transitions from the lowest excited triplet state, T_1 , to the ground singlet state, S_0 . Because phosphorescence undergoes a spin-forbidden transition, the lifetimes of phosphorescence (10^{-6} – 10^2 s) are normally longer than those of fluorescence (10^{-9} – 10^{-7} s). Interference from any fluorescent emission and scattering light can be easily avoided by using an appropriate delay time.^{19,20} In addition, main advantage of phosphorescence imaging compared to the fluorescence imaging is its larger Stokes' shift that results in obvious spectral separation between the phosphorescence emission and the excitation light. The use of RTP as a sensing system requires a suitable phosphorescence indicator for a given analyte. A general strategy for the design of new RTP-sensing systems is based on phosphorescence energy transfer (PET), an energy-transfer process in which the phosphorescent molecule (donor) transfers its energy to an absorber (acceptor) at close proximity through dipole–dipole coupling of the donor and acceptor molecules.^{21–23}

Received: September 30, 2015

Accepted: November 5, 2015

Published: November 5, 2015

Herein, we describe the design, properties, and NQO1-specific cellular activation of a PET probe, quinone-capped Mn-doped ZnS QDs (Q-Mn:ZnS QDs), for NQO1-specific detection. Mn-doped ZnS quantum dots (Mn:ZnS QDs)^{24–28} function as donors and trimethylquinone propionic acids (QPA) are the acceptors; the phosphorescence of Mn:ZnS QDs is quenched through PET from Mn:ZnS QDs to covalently bonded quinones. The phosphorescence of Mn:ZnS QDs is turned on by the rapid removal of the quinone quencher by NQO1, which catalyzes the reduction of quinones to hydroquinones with electrons provided by NADH. The Q-Mn:ZnS QD probe shows low cellular toxicity and can rapidly distinguish between NQO1-expressing and -nonexpressing cancer cell lines through phosphorescence imaging.

■ EXPERIMENTAL SECTION

Materials and Reagents. Recombinant human NQO1 (NQO1) and $\text{Zn}(\text{BF}_4)_2 \cdot x\text{H}_2\text{O}$ were purchased from Sigma-Aldrich. 2,3,5-Trimethylhydroquinone, 3,3-dimethylacrylic acid, methanesulfonic acid, *N*-bromosuccinimide, 1,3-dicyclohexylcarbodiimide, and *N,N*-(dimethylamino)pyridine, were purchased from Alfa Aesar. $\text{MnSO}_4 \cdot \text{H}_2\text{O}$ and $\text{H}_2\text{S} \cdot 9\text{H}_2\text{O}$ were purchased from Riedel-de Haen. All the other materials were analytically pure and were used without further purification. For all aqueous solutions, deionized water (resistivity, 18.0 $\text{M}\Omega \cdot \text{cm}$ at 25 °C) purified by Millipore Direct-Q water purification unit was used. The synthesis and characterization of 3-methyl-3-(2,4,5-trimethyl-3,6-dioxocyclohexa-1,4-dienyl)butanoic acid²⁹ and *N*-hydroxysuccinimidyl ester are described in the Supporting Information.

Instruments. NMR spectra were obtained on Bruker DRX-300 NMR (Billerica, Massachusetts, USA). Phosphorescence spectra were recorded on Hitachi F-7000 fluorescence spectrometer (Tokyo, Japan). TEM images were recorded from JEOL JEM-2010 transmission electron microscope (Tokyo, Japan). IR spectra were recorded on Bomem DA8.3 Fourier transform spectrometer (Quebec, Canada). Cyclic voltammograms were recorded on a CHI 600D electrochemical analyzer (Austin, USA). Fluorescent pictures were taken on a Leica TCS-SP5-X AOBs confocal fluorescence microscope. Time-resolved photoluminescence of Mn:ZnS QDs was done by a tunable Nd:YAG-laser system NT342/1/UV, EKSPLA, Lithuania.

Synthesis of Q-Mn:ZnS QDs. Mn-doped ZnS quantum dots were synthesized in the aqueous solution at room temperature by chemical coprecipitation.^{21,30} To 800 μL of $\text{DI-H}_2\text{O}$ in an enppendorff were added 100 μL of 0.1 M $\text{Zn}(\text{BF}_4)_2$ aqueous solution and 5 μL of 0.1 M MnSO_4 aqueous solution. After 10 min, 100 μL of $\text{Na}_2\text{S} \cdot 9\text{H}_2\text{O}$ aqueous solution (0.1 M) was added into the above solution. The mixture solution was mixed totally and put in the sonication bath for 2 h. Mn:ZnS QDs powders were obtained after centrifugation and washed three times with $\text{DI-H}_2\text{O}$ to remove excess reactants. 2-Mercaptoethanol-capped Mn:ZnS QDs were formed by adding 20 μL of 2-mercaptoethanol to the solution containing Mn:ZnS QDs. The mixture solution was sonicated overnight to get the 2-mercaptoethanol capped on the surface of Mn:ZnS QDs. Then, 2-mercaptoethanol-capped Mn:ZnS QDs were obtained, after being centrifuged and washed three times with ethanol to remove unbound 2-mercaptoethanol.

$\text{H}_2\text{N-Mn:ZnS}$ QDs were obtained by adding (3-aminopropyl)triethoxysilane (APTES, 25 μL) to the solution containing 2-mercaptoethanol-capped Mn:ZnS QDs in

ethanol. The mixture was stirred for 30 min. $\text{NH}_3 \cdot \text{H}_2\text{O}$ (0.625 mL 6%) was added into the above solution and stirred at room temperature overnight. After the formation of the silica shell, the white suspension was spun down and washed twice with ethanol and three times with $\text{DI-H}_2\text{O}$. $\text{H}_2\text{N-Mn:ZnS}$ QDs were obtained for further using.

Q-Mn:ZnS QDs were prepared by adding 200 μL of 3-methyl-3-(2,4,5-trimethyl-3,6-dioxocyclohexa-1,4-dienyl)butanoic acid, *N*-hydroxysuccinimidyl ester (0.14 M in THF), and 6 μL of triethylamine to the solution containing $\text{H}_2\text{N-Mn:ZnS}$ quantum dots. The mixture was heated at 80 °C for 12 h, and then the yellow pellets were yielded. The yellow pellets were washed three times with ethanol and $\text{DI-H}_2\text{O}$. Q-Mn:ZnS QDs were obtained and stored in the dark for further use.

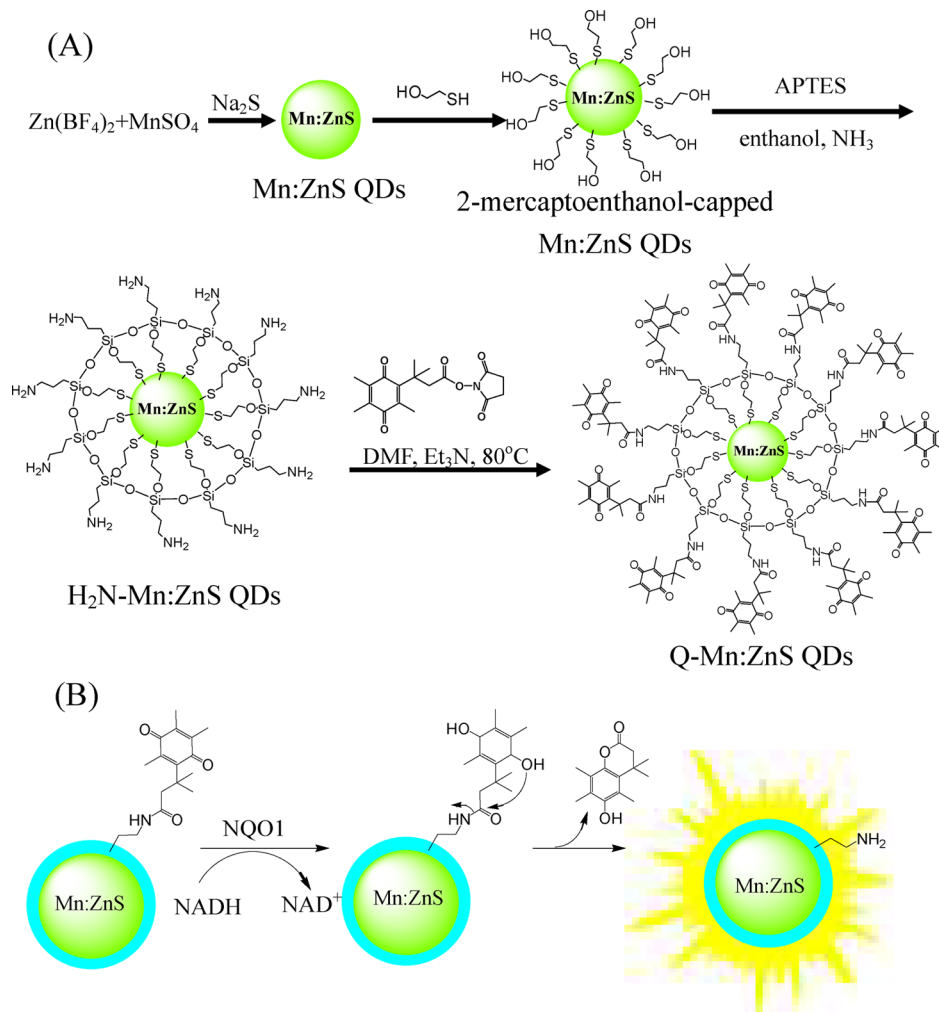
NQO1 Detection by Q-Mn:ZnS QDs. To 200 μL of Q-Mn:ZnS QDs (0.25 mg mL^{-1}) in phosphate-buffered saline buffer (1X PBS (pH 7.4), containing 137 mM NaCl, 2.7 mM KCl, 10 mM Na_2HPO_4 , and 2 mM KH_2PO_4) were added different analytes (BSA, catalase, cysteine, cytochrome C, GOx, GSH, Hcys, IgG, lysozyme, NADH, NQO1, SOD, tyrosinase), respectively. The mixtures were incubated at room temperature for 30 min. For the phosphorescence measurement, the excitation wavelength was 316 nm and the emission intensities were recorded at 590 nm by fluorescence spectrometer.

Enzyme Kinetic Assay. The enzyme kinetic assay was obtained from the phosphorescence measurement ($\lambda_{\text{ex}} = 316$ nm, $\lambda_{\text{em}} = 590$ nm). The concentrations of Q-Mn:ZnS QDs were from 0.25 to 1.9 mg mL^{-1} . NQO1 (0.01 g L^{-1} , 3.23×10^{-7} M) was added to the solution containing Q-Mn:ZnS QDs and NADH (10^{-4} M) in 10 mM PBS with 0.007% BSA. The time for the reaction was 10 min at room temperature. Phosphorescence intensity was converted to concentration according to the phosphorescent intensity of the known concentration of $\text{H}_2\text{N-Mn:ZnS}$ QDs. The values of Michaelis constant (K_m) and catalytic constant (k_{cat}) were obtained from the Lineweaver–Burk plot of Q-Mn:ZnS QDs. The intercept on the x axis is $1/K_m$; the intercept on the y axis is $1/V_{\text{max}}$. The value of the catalytic constant (k_{cat}) is obtained from the equation: $V_{\text{max}} = k_{\text{cat}} [\text{E}]$.

Cell Culture for A549, HCT-116, MCF-7, and HL-60 Cell Lines. The cell lines A549, HCT-116, MCF-7, and HL-60 cell were provided by the Food Industry Research and Development Institute (Taiwan). A549, HCT-116, and MCF-7 cell lines were cultured in DMEM medium (Dulbecco's Modified Eagle's Medium, high glucose), and 10% fetal bovine serum (FBS) with 100 mg L^{-1} kanamycin-streptomycin. HL-60 cell line was cultured in RPMI 1640 medium and 10% fetal bovine serum (FBS) with 100 mg L^{-1} kanamycin-streptomycin. The cell lines were incubated at 37 °C under an atmosphere of 5% CO_2 .

Cytotoxicity Assay. A549 cells were seeded in a 96-well plate with 200 μL of DMEM medium supplemented with 10% fetal bovine serum (FBS) and 0.1 g L^{-1} kanamycin-streptomycin and incubated in 5 wt % CO_2 at 37 °C overnight. The cells were treated with different concentrations of Q-Mn:ZnS QDs in the DMEM medium. After incubation overnight, the medium was removed and 200 μL of 3-(4,5-dimethylthiazol-2-yl)-2,5-diphenyltetrazolium bromide (MTT) solution (5 mg mL^{-1} in 1X PBS buffer, pH 7.4) was added to each well for 4 h of incubation. Following removal of MTT solution, the observed yellow precipitates (formazan) in plates were dissolved in 200 μL of DMSO and 25 μL of Sorenson's glycine buffer (0.1 M glycine and 0.1 M NaCl). A Multiskan

Scheme 1. (A) Synthesis of Q-Mn:ZnS QDs. (B) Activation of Q-Mn:ZnS QDs by NQO1 to yield phosphorescence



GO microplate reader was used to measure the absorbance at 570 nm for each well. The viability of cells was calculated according to the following equation:

$$\text{cell viability(\%)} = \frac{(\text{mean of absorbance value of treatment group})}{(\text{mean of absorbance value of control group})}$$

Imaging of NQO1 in Living Cells. Experiments to assess the sensing ability of Q-Mn:ZnS QDs for exogenous NQO1 were performed in 1X PBS (pH 7.4). A549 cell line and HL-60 cell line were seeded on $20 \times 20 \text{ mm}^2$ glass coverslips in DMEM medium and gelatin-coated glass coverslips in RPMI 1640 medium, respectively. The cell lines were cultured in the incubation medium supplemented with 10% fetal bovine serum (FBS) and 0.1 g L^{-1} kanamycin-streptomycin in 6-well plates in 5 wt % vol CO_2 at 37°C overnight to get suitable density. Then, the cell lines were incubated in the medium with 0.25 mg mL^{-1} Q-Mn:ZnS QDs for 1 h and washed with 1X PBS buffer three times to remove excess Q-Mn:ZnS QDs. Confocal fluorescence imaging of cells was performed with a Leica TCS SP5 X AOBs confocal fluorescence microscope (Germany), and a $100\times$ oil-immersion objective lens was used. The cells were excited with a white light laser at 405 nm, and emission was collected at 575–605 nm.

RESULTS AND DISCUSSION

Characterization of Q-Mn:ZnS QDs. The synthesis of Q-Mn:ZnS QDs is outlined in Scheme 1. First, the synthesis of Mn:ZnS QDs was carried out through the reaction of zinc tetrafluoroborate and manganese sulfate with sodium sulfide according to a previously reported procedure.^{21,30} 2-Mercaptoethanol was then used to modify the surface of the Mn:ZnS QDs. H₂N-Mn:ZnS QDs were obtained by addition of (3-aminopropyl)triethoxysilane to a solution of dispersed quantum dots to form a silica shell on the surface of Mn:ZnS QDs. Q-Mn:ZnS QDs were prepared by modification of H₂N-Mn:ZnS QDs with quinone derivatives.

Transmission electron microscopy images reveal that the average particle size of Q-Mn:ZnS QDs is about $6.0 \pm 0.2 \text{ nm}$ (Figure 1). Q-Mn:ZnS QDs were also characterized by infrared spectroscopy. In Figure 2B, the peak at 3450 cm^{-1} represents typical O–H stretching, indicating that mercaptoethanol is bound to the quantum dots. In Figure 2C, the characteristic peaks of H₂N-Mn:ZnS QDs are at 2929, 2878, 1130 (Si–O), and 1028 cm^{-1} (Si–O).^{31,32} In Figure 2D, the peak at 1666 cm^{-1} represents typical strong carbonyl (C=O) stretching,³³ indicating that quinone species are bound to the quantum dots via the amide bond.

Phosphorescence Quenching of Q-Mn:ZnS QDs through the PET Mechanism. To further confirm that the

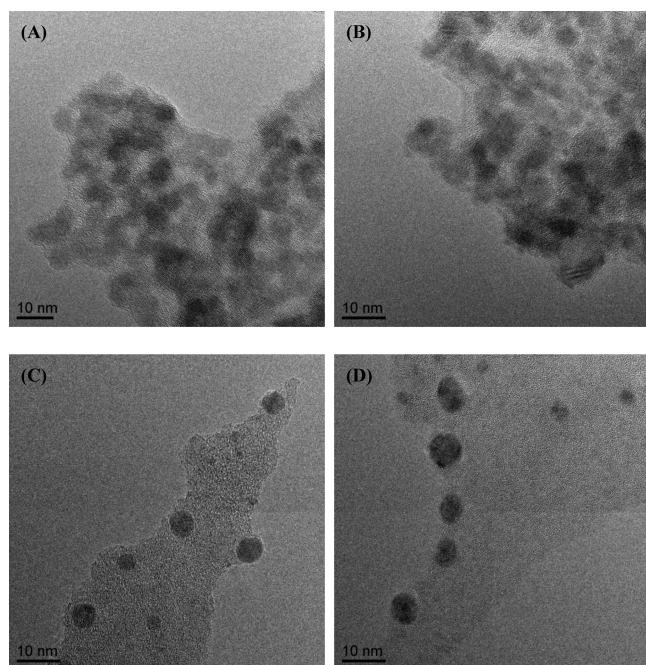


Figure 1. TEM images of (A) Mn:ZnS QDs, (B) 2-mercaptoethanol-Mn:ZnS QDs, (C) H₂N-Mn:ZnS QDs, and (D) Q-Mn:ZnS QDs.

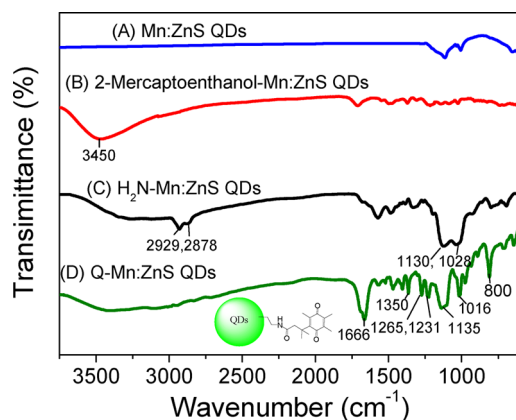


Figure 2. FT-IR spectra of (A) Mn:ZnS QDs, (B) 2-mercaptoethanol-Mn:ZnS QDs, (C) H₂N-Mn:ZnS QDs, and (D) Q-Mn:ZnS QDs.

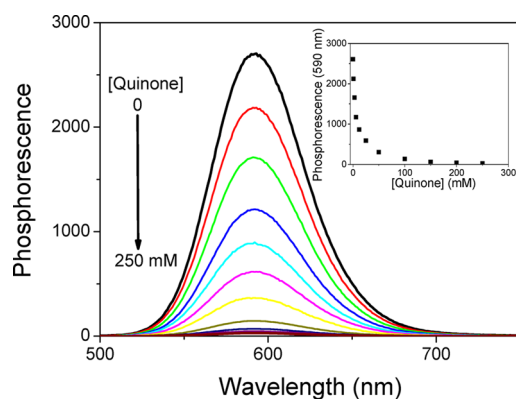


Figure 3. Phosphorescence quenching of H₂N-Mn:ZnS QDs with varying amounts of quinone modified.

quenching mechanism of Q-Mn:ZnS QDs is PET, phosphorescence spectra of H₂N-Mn:ZnS QDs were obtained in the

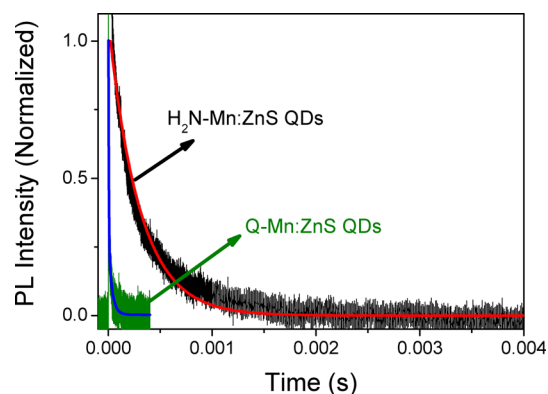


Figure 4. Time-resolved photoluminescence recorded at 590 nm of Mn:ZnS QDs. Data for H₂N-Mn:ZnS QDs and Q-Mn:ZnS QDs are shown in black and green, respectively. The phosphorescence decay was recorded at room temperature with pulsed excitation at 355 nm.

Table 1. Parameters for Time-Resolved Phosphorescence Decays of Q-Mn:ZnS QDs

compound	τ_{avg} (μs) ^a	k_{ET} (s^{-1}) ^b
H ₂ N-Mn:ZnS QDs	546 ± 0.7	
Q-Mn:ZnS QDs	24.6 ± 0.4	3.88 × 10 ⁴

^aThe average lifetime is calculated by using the statistical definition in eq 3. ^bThe energy-transfer rate was estimated by using eq 6.

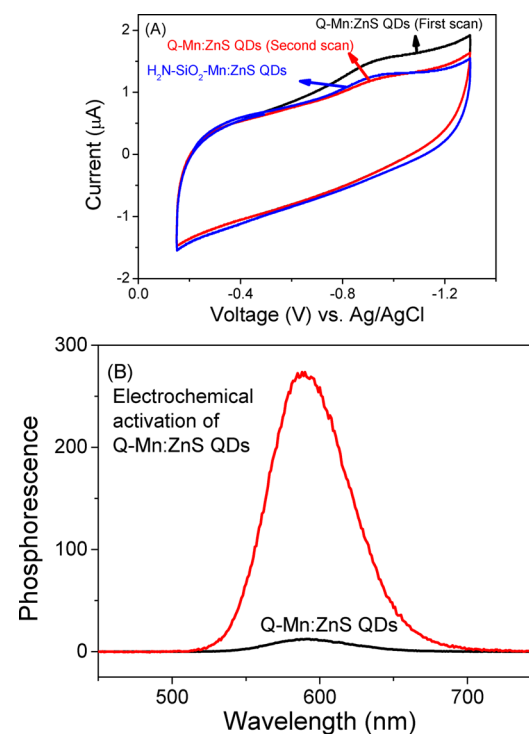


Figure 5. (A) Cyclic voltammograms for Q-Mn:ZnS QDs. The electrochemical activation of Q-Mn:ZnS QDs. The black trace is of the first scan, and the red traces are of two subsequent scans, indicating nearly complete conversion of quinone to hydroquinone during the first scan. (B) Phosphorescence spectra of Q-Mn:ZnS QDs with and without electrochemical activation.

presence of different concentrations of quinone derivatives (0–250 mM). The phosphorescence intensities decreased when more quinones were modified on the quantum dots (Figure 3).

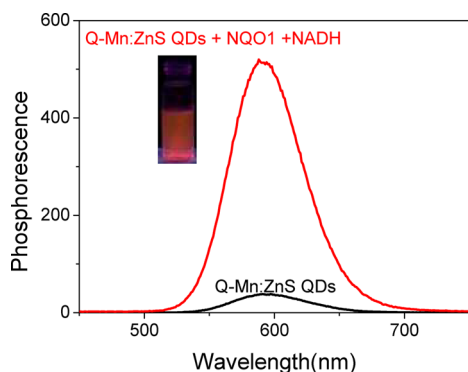


Figure 6. Phosphorescence spectra of Q-Mn:ZnS QDs (0.25 mg mL^{-1}) and Q-Mn:ZnS QDs (0.25 mg mL^{-1}) reacted with NQO1 ($0.32 \text{ }\mu\text{M}$) and NADH (0.1 mM).

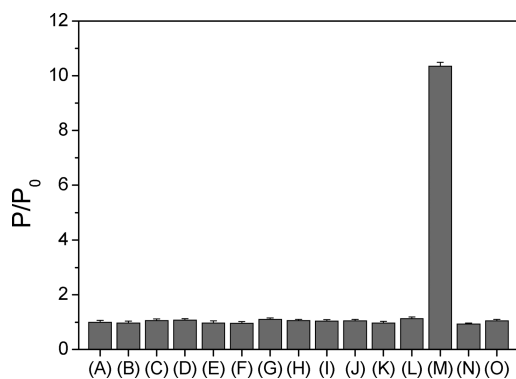


Figure 7. Selectivity of the Q-Mn:ZnS QDs for NQO1 detection by comparison with the other species. The species are (A) Q-Mn:ZnS QDs, (B) BSA, (C) catalase, (D) cysteine, (E) cytochrome C, (F) glucose oxidase, (G) GSH, (H) Hcy, (I) IgG, (J) lysozyme, (K) NADH, (L) NQO1, (M) NQO1+NADH, (N) SOD, and (O) tyrosinase. Experiments were performed in 1X PBS buffer containing NADH (0.1 mM) and 0.007% BSA at room temperature with the excitation wavelength 316 nm in the presence of 0.25 mg mL^{-1} Q-Mn:ZnS QDs.

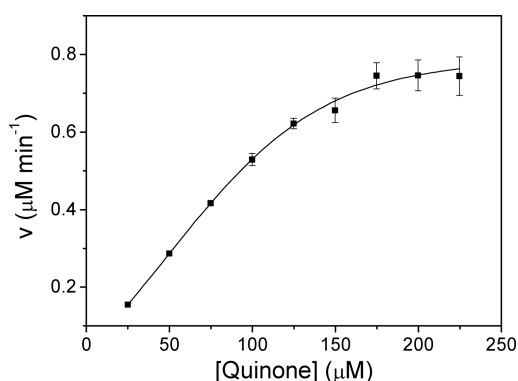


Figure 8. Kinetics of the reduction of Q-Mn:ZnS QDs by NQO1. All of the experiments were measured in NADH (0.1 M) and NQO1 ($10^{-2} \text{ }\mu\text{g }\mu\text{L}^{-1}$, $0.32 \text{ }\mu\text{M}$) in pH 7.4, 1X PBS buffer with 0.007% BSA. Excitation wavelength 316 nm and emission wavelength 590 nm . Values ($n = 3$) are the average ± 1 standard deviation.

The maximum quenching efficiency reached 98% upon addition of 200 mM quinone derivatives.

To determine the quenching mechanism (dynamic quenching or static quenching), two equations, Stern–Volmer's

equation (eq 1) and the Lineweaver–Burk equation (eq 2), are used.¹⁹

$$P_0/P = 1 + K_{sv}c_q \quad (1)$$

$$P_0/(P_0 - P) = 1 + K_{LB}/c_q \quad (2)$$

P_0 and P are the phosphorescence of the quantum dots without and with quinone modification, respectively, and c_q is the concentration of quinone species. K_{sv} is the dynamic quenching constant, and K_{LB} is the static quenching constant. As the relationship between P_0/P and the concentration of QPA does not follow the Stern–Volmer's equation, the quenching mechanism is not dynamic quenching (Figure S2, Supporting Information). In addition, the relationship between $P_0/(P_0 - P)$ and the QPA concentration from 0 to 200 mM follows the Lineweaver–Burk equation, indicating that the quenching mechanism is a static quenching system. Quenching of Q-Mn:ZnS QDs via the PET quenching mechanism suggests that energy was transferred from the quantum dots to the quinone species.

Time-resolved photoluminescence of Mn:ZnS QDs was carried out to elucidate the energy-transfer dynamics in the Q-Mn:ZnS QDs system. First, the spectral overlap between the emission of Mn:ZnS QDs and the absorption of quinone is added to Figure S1 in the Supporting Information. Figure S1 shows that the emission spectrum of Mn:ZnS QDs overlaps with the absorption spectrum of QPA, suggesting that PET between Mn:ZnS QDs and QPA can happen. According to the PET process, Mn:ZnS QDs act as donors, whereas QPA act as acceptors (quenchers) in this system. In addition, Figure 4 shows time-resolved phosphorescence transients for Q-Mn:ZnS QDs and $\text{NH}_2\text{-Mn:ZnS QDs}$. To compare the phosphorescence decays between two Mn:ZnS QDs, the average phosphorescence lifetime is calculated as follows:

$$\tau_{\text{avg}} \equiv \frac{\int tI(t) dt}{\int I(t) dt} \approx \frac{\sum A_i \tau_i^2}{\sum A_i \tau_i} \quad (3)$$

where A_i and τ_i represent the amplitude and the lifetime of each component, respectively. In the $\text{NH}_2\text{-Mn:ZnS QDs}$ system, the reciprocal of the average phosphorescence lifetime is the sum of the radiative (k_r) and nonradiative (k_{nr}) rate coefficients:

$$1/\tau_{(\text{NH}_2\text{-Mn:ZnS QDs})} = k_r + k_{nr} \quad (4)$$

In the Q-Mn:ZnS QD system, the average phosphorescence lifetime decreases significantly because of the contribution of energy transfer from the Mn:ZnS QDs to the quinone species. Thus, the average phosphorescence lifetime for Q-Mn:ZnS QDs is given by

$$1/\tau_{(\text{Q-Mn:ZnS QDs})} = k_r + k_{nr} + k_{ET} \quad (5)$$

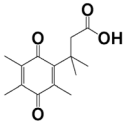
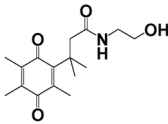
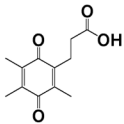
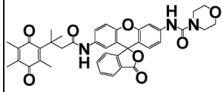
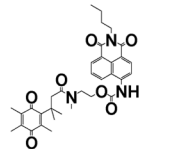
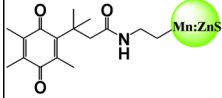
where k_{ET} is the rate of energy transfer from the Mn:ZnS QDs to the quinone species. Equations 4 and 5 give the expression

$$k_{ET} = 1/\tau_{(\text{Q-Mn:ZnS QDs})} - 1/\tau_{(\text{NH}_2\text{-Mn:ZnS QDs})} \quad (6)$$

As shown in Table 1, the rate of energy transfer from Mn:ZnS QDs to the quinone species is $3.88 \times 10^4 \text{ s}^{-1}$. Results from time-resolved photoluminescence strongly suggest that phosphorescence energy is transferred from the Mn:ZnS QDs to the quinone species.

To test the modification with electroactive quinones on Q-Mn:ZnS QDs, cyclic voltammetry was applied in the measure-

Table 2. Kinetic Parameters for the Reduction of Quinone Species by NQO1

Quinone	V_{\max} ($\frac{\mu\text{mol}}{\text{min}\cdot\text{mgNQO1}}$)	K_m (μM)	k_{cat} (s^{-1})	k_{cat}/K_m ($\text{M}^{-1}\text{s}^{-1}$)	Ref.
	38 ± 5	158 ± 41	20 ± 3	$1.2 \pm 0.4 \times 10^5$	34
	60 ± 7	132 ± 32	31 ± 4	$2.3 \pm 0.6 \times 10^5$	34
	66 ± 4	5 ± 1	34 ± 2	$6.8 \pm 1.4 \times 10^6$	34
	$2.1 \pm 0.1 \times 10^{-3}$	23.7 ± 3.5	$2.2 \pm 1.3 \times 10^{-3}$	93 ± 15	17
	$3.7 \pm 0.2 \times 10^{-2}$	3.9 ± 0.8	$1.9 \pm 0.1 \times 10^{-2}$	$4.9 \pm 0.3 \times 10^3$	4
	$2.2 \pm 0.1 \times 10^{-1}$	325 ± 14	$1.1 \pm 0.1 \times 10^{-1}$	346 ± 5	This method

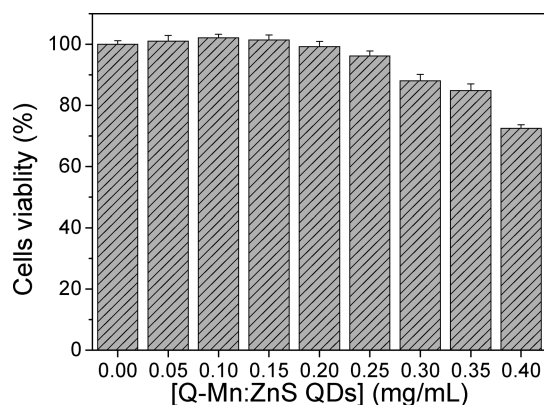


Figure 9. Cell viability in the presence of different concentrations of Q-Mn:ZnS QDs. A549 cells were cultured in the presence of Q-Mn:ZnS QDs (0–0.40 mg/mL) in the DMEM medium at 37 °C for 12 h. Three measurements were done for each concentration of Q-Mn:ZnS QDs.

ment of Q-Mn:ZnS QDs in 1X PBS buffer. The prominent cathodic peak in the first scan proves the presence of

electroactive quinones on the Q-Mn:ZnS QDs.²⁹ The profile of the Q-Mn:ZnS QDs for the second scan is not the same as that for as the first scan, but identical to that of H₂N–Mn:ZnS QDs (Figure 5). When the potentials were below –0.9 V, the quinone species on the surface of Mn:ZnS QDs underwent reduction to hydroquinones and subsequent intramolecular cyclization reaction, resulting in removal of quinone from the Mn:ZnS QDs in the first scan. After electrochemical reduction, phosphorescence of the Q-Mn:ZnS QD solution is turned on because of the release of the quencher, quinone.

Phosphorescence Generation by Q-Mn:ZnS QDs upon NQO1 Detection. The sensing ability of Q-Mn:ZnS QDs for NQO1 was then tested. NQO1 could reduce quinones to hydroquinones. The subsequent intramolecular cyclization reaction removes the quencher from the Q-Mn:ZnS QDs and results in removal of quinone from the Mn:ZnS QDs (Scheme 1). Phosphorescence of Q-Mn:ZnS QDs is then turned on. As shown in Figure 6, the phosphorescence intensity showed a 10-fold increase after the reaction of Q-Mn:ZnS QDs with NQO1 and NADH for 30 min. The significant difference in phosphorescence sufficiently demonstrates this method as an off–on phosphorescence system for NQO1 detection.

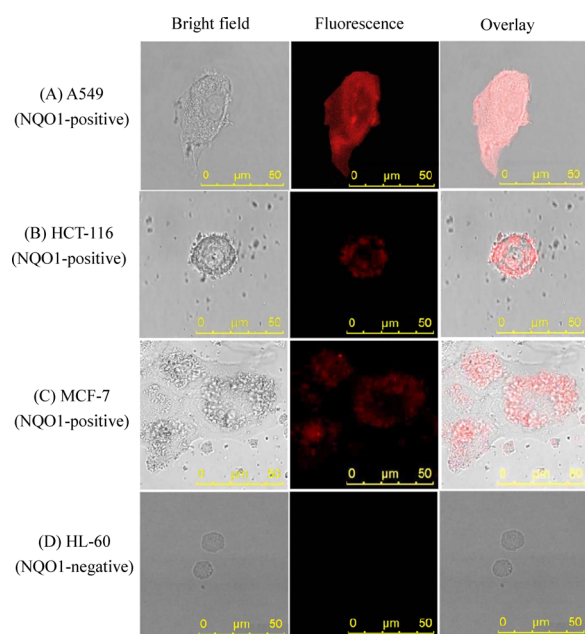


Figure 10. Images of NQO1 detection with Q-Mn:ZnS QDs. (A) A549 cells, (B) HCT-116 cells, (C) MCF-7 cells, and (D) HL-60 cells were incubated with Q-Mn:ZnS QDs for 1 h, respectively.

To test the selectivity of the Q-Mn:ZnS QDs, several proteins and amino acids were tested. In Figure 7, only NQO1 shows a high phosphorescence intensity ratio (P/P_0); the other proteins did not cause any change in the P/P_0 value. Q-Mn:ZnS QDs showed high selectivity to NQO1.

Kinetic Study of Q-Mn:ZnS QDs with NQO1. The catalytic ability of NQO1 to activate Q-Mn:ZnS QDs was investigated by using a kinetic assay. Figure 8 shows a Michaelis–Menten plot of the reduction of Q-Mn:ZnS QDs by NQO1. The kinetic parameters obtained from the Michaelis–Menten plot in Figure 8 are shown in Table 2. Q-Mn:ZnS QDs yielded a catalytic constant (k_{cat}) higher than those of the other organic probes for NQO1 detection.^{4,17,34} Moreover, the K_m value of the Q-Mn:ZnS QDs is larger than that of most quinones because of the large volume of QDs.

Imaging of NQO1 in Living Cells. The potential of the Q-Mn:ZnS QD probe for imaging NQO1 in living cells was investigated. A MTT assay was conducted with a A549 cell line to evaluate the cytotoxicity of the probe. In Figure 9, the estimated cellular viability after 24 h is greater than 80%, which

indicates that the Q-Mn:ZnS QDs ($<0.35 \text{ mg mL}^{-1}$) have low cytotoxicity. Furthermore, images of the cells were obtained by using a confocal fluorescence microscope. NQO1-positive cell lines such as A549,⁴ HCT-116,³⁵ and MCF-7,³⁶ as well as the NQO1-negative cell line HL-60³⁷ were treated with Q-Mn:ZnS QDs. As shown in Figure 10, red emissions were observed in the A549, HCT-116, and MCF-7 cells. This observation indicates that NQO1 expression occurs in these cells. On the contrary, no red emission was observed in the HL-60 cell line. Because HL-60 cells are NQO1-negative,³⁷ Q-Mn:ZnS QDs were not activated in the HL-60 cells. Q-Mn:ZnS QDs could specifically detect NQO1 expression in living cells. To determine the subcellular localization of endogenous NQO1 using the Q-Mn:ZnS QDs probe, a Hoechst nuclear stain was used. Figure 11 shows that the color change caused by the Q-Mn:ZnS QD probe does not overlap with that caused by the Hoechst stain. This observation indicates that there were no Q-Mn:ZnS QDs staining in the nuclear region and that Q-Mn:ZnS QD probe may be used to detect endogenous NQO1 in the cytosol.

CONCLUSION

We have developed a phosphorescence turn-on probe for NQO1 using Q-Mn:ZnS QDs. Quinones on the surface of the Q-Mn:ZnS QDs were reduced to hydroquinones by NQO1 and then removed from the surface; red phosphorescence of Mn:ZnS QDs was then turned on. Cells expressing NQO1 could be selectively detected by the Q-Mn:ZnS QD probe. Q-Mn:ZnS QDs could be used to distinguish NQO1-positive cell lines from NQO1-negative cell lines. The cytotoxicity assay showed that the NQO1 probe has low cellular toxicity. Q-Mn:ZnS QDs can be a useful NQO1 probe for detecting cancer cells expressing NQO1.

ASSOCIATED CONTENT

Supporting Information

The Supporting Information is available free of charge on the ACS Publications website at DOI: 10.1021/acsami.5b09244.

Synthesis and characterization of 3-methyl-3-(2,4,5-trimethyl-3,6-dioxocyclohexa-1,4-dienyl) butanoic acid and hydroxysuccinimidyl ester. Figures S1–S9: spectral overlay of phosphorescence spectrum, Stern–Volmer and Lineweaver–Burk plots, phosphorescent signal, ¹H NMR spectra, EI-MS spectra (PDF)

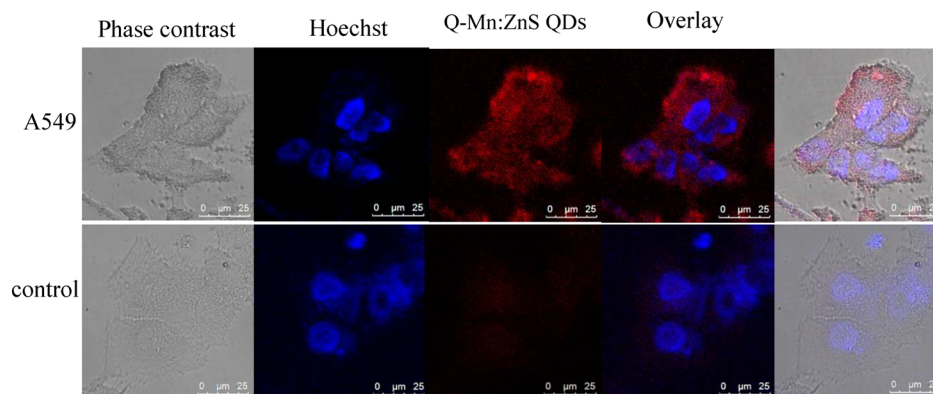


Figure 11. Images of NQO1 detection with Q-Mn:ZnS QDs. A549 cells were incubated with Q-Mn:ZnS QDs for 1 h.

AUTHOR INFORMATION

Corresponding Author

*S.-P. Wu. Tel: +886-3-5712121, ext 56506. Fax: +886-3-5723764. E-mail: spwu@mail.nctu.edu.tw.

Notes

The authors declare no competing financial interest.

ACKNOWLEDGMENTS

We gratefully acknowledge the financial support of Ministry of Science and Technology (Taiwan) for supporting this research under the grant (MOST 104-2113-M-009-011) and National Chiao Tung University.

REFERENCES

- (1) Kobayashi, H.; Choyke, P. L. Target-Cancer-Cell-Specific Activatable Fluorescence Imaging Probes: Rational Design and in Vivo Applications. *Acc. Chem. Res.* **2011**, *44*, 83–90.
- (2) Zhang, H.; Fan, J.; Wang, J.; Zhang, S.; Dou, B.; Peng, X. An Off-On COX-2-Specific Fluorescent Probe: Targeting the Golgi Apparatus of Cancer Cells. *J. Am. Chem. Soc.* **2013**, *135*, 11663–11669.
- (3) Uddin, M. J.; Crews, B. C.; Ghebreselasie, K.; Marnett, L. J. Design, Synthesis, and Structure–Activity Relationship Studies of Fluorescent Inhibitors of Cyclooxygenase-2 as Targeted Optical Imaging Agents. *Bioconjugate Chem.* **2013**, *24*, 712–723.
- (4) Silvers, W. C.; Prasai, B.; Burk, D. H.; Brown, M. L.; McCarley, R. L. Profluorogenic Reductase Substrate for Rapid, Selective, and Sensitive Visualization and Detection of Human Cancer Cells that Overexpress NQO1. *J. Am. Chem. Soc.* **2013**, *135*, 309–314.
- (5) Schlager, J. J.; Hoerl, B. J.; Riebow, J.; Scott, D. P.; Gaskaska, P.; Scott, R. E.; Powis, G. Increased NAD(P)H:(Quinone-Acceptor)-Oxidoreductase Activity Is Associated with Density-dependent Growth Inhibition of Normal but not Transformed Cells. *Cancer Res.* **1993**, *53*, 1338–1342.
- (6) Danson, S.; Ward, T. H.; Butler, J.; Ranson, M. DT-diaphorase: a Target for New Anticancer Drugs. *Cancer Treat. Rev.* **2004**, *30*, 437–449.
- (7) Faig, M.; Bianchet, M. A.; Talalay, P.; Chen, S.; Winski, S.; Ross, D.; Amzel, L. M. Structures of Recombinant Human and Mouse NAD(P)H:quinone oxidoreductases: Species Comparison and Structural Changes with Substrate Binding and Release. *Proc. Natl. Acad. Sci. U. S. A.* **2000**, *97*, 3177–3182.
- (8) Cresteil, T.; Jaiswal, A. K. High Levels of Expression of the NAD(P)H: Quinone Oxidoreductase (NQO1) Gene in Tumor Cells Compared to Normal Cells of the Same Origin. *Biochem. Pharmacol.* **1991**, *42*, 1021–1027.
- (9) Malkinson, A. M.; Siegel, D.; Forrest, G. L.; Gazdar, A. F.; Oie, H. K.; Chan, D. C.; Bunn, P. A.; Mabry, M.; Dykes, D. J.; Harrison, S. D.; Ross, D. Elevated DT-diaphorase Activity and Messenger RNA Content in Human Non-Small Cell Lung Carcinoma: Relationship to the Response of Lung Tumor Xenografts to Mitomycin C. *Cancer Res.* **1992**, *52*, 4752–4757.
- (10) Ross, D.; Kepa, J. K.; Winski, S. L.; Beall, H. D.; Anwar, A.; Siegel, D. NAD(P)H:quinone Oxidoreductase 1 (NQO1): Chemoprotection, Bioactivation, Gene Regulation and Genetic Polymorphisms. *Chem.-Biol. Interact.* **2000**, *129*, 77–97.
- (11) Edlund, C.; Elhammer, A.; Dallner, G. Distribution of Newly Synthesized DT-diaphorase in Rat Liver. *Biosci. Rep.* **1982**, *2*, 861–865.
- (12) Prochaska, H. J.; Fernandes, C. L. Elevation of Serum Phase II Enzymes by Anticarcinogenic Enzyme Inducers: Markers for a Chemoprotected State? *Carcinogenesis* **1993**, *14*, 2441–2445.
- (13) Nakamura, M.; Hayashi, T. One- and Two-Electron Reduction of Quinones by Rat Liver Subcellular Fractions. *J. Biochem.* **1994**, *115*, 1141–1147.
- (14) Sreerama, L.; Hedge, M. W.; Sladek, N. E. Identification of a Class 3 Aldehyde Dehydrogenase in Human Saliva and Increased Levels of This Enzyme, Glutathione S-transferases, and DT-diaphorase

in the Saliva of Subjects Who Continually Ingest Large Quantities of Coffee or Broccoli. *Clin. Cancer Res.* **1995**, *1*, 1153–1163.

(15) Appelt, L. C.; Reicks, M. M. Soy Induces Phase II Enzymes But Does Not Inhibit Dimethylbenz[a]anthracene-Induced Carcinogenesis in Female Rats. *J. Nutr.* **1999**, *129*, 1820–1826.

(16) Das, M.; Rastogi, S.; Khanna, S. K. Mechanism to Study 1:1 Stoichiometry of NADPH and Alkoxyphenoxazones Metabolism Spectrophotometrically in Subcellular Biological preparations. *Biochim. Biophys. Acta, Gen. Subj.* **2004**, *1675*, 1–11.

(17) Silvers, W. C.; Payne, A. S.; McCarley, R. L. Shedding Light by Cancer redox—human NAD(P)H:quinone Oxidoreductase 1 Activation of a Cloaked Fluorescent Dye. *Chem. Commun.* **2011**, *47*, 11264–11266.

(18) Sanchez-Barragan, I.; Costa-Fernández, J.; Sanz-Medel, A.; Valledor, M.; Campo, J. Room-Temperature Phosphorescence (RTP) for Optical Sensing. *TrAC, Trends Anal. Chem.* **2006**, *25*, 958–967.

(19) He, Y.; Wang, H. F.; Yan, X. P. Exploring Mn-Doped ZnS Quantum Dots for the Room-Temperature Phosphorescence Detection of Enoxacin in Biological Fluids. *Anal. Chem.* **2008**, *80*, 3832–3837.

(20) Yan, H.; Wang, H. F. Turn-on Room Temperature Phosphorescence Assay of Heparin with Tunable Sensitivity and Detection Window Based on Target-Induced Self-Assembly of Polyethyleneimine Capped Mn-Doped ZnS Quantum Dots. *Anal. Chem.* **2011**, *83*, 8589–8595.

(21) Zhang, L.; Cui, P.; Zhang, B.; Gao, F. Aptamer-Based Turn-On Detection of Thrombin in Biological Fluids Based on Efficient Phosphorescence Energy Transfer from Mn-Doped ZnS Quantum Dots to Carbon Nanodots. *Chem. - Eur. J.* **2013**, *19*, 9242–9250.

(22) Zhang, L.; Zhang, R.; Cui, P.; Cao, W.; Gao, F. An Efficient Phosphorescence Energy Transfer Between Quantum Dots and Carbon Nanotubes For Ultrasensitive Turn-on Detection of DNA. *Chem. Commun.* **2013**, *49*, 8102–8104.

(23) Chang, C.; Lee, R.; Diau, E. W. Energy Transfer And Phosphorescence-quenching Dynamics in a Phosphorescent Host-guest System. *Chem. Phys. Lett.* **2013**, *561–562*, 52–56.

(24) Wang, X.; Xu, J.; Chen, H. A New Electrochemiluminescence Emission of Mn²⁺-Doped ZnS Nanocrystals in Aqueous Solution. *J. Phys. Chem. C* **2008**, *112*, 17581–17585.

(25) Wang, H.; Li, Y.; Wu, Y.; He, Y.; Yan, X. Ascorbic Acid Induced Enhancement of Room Temperature Phosphorescence of Sodium Tripolyphosphate-Capped Mn-Doped ZnS Quantum Dots: Mechanism and Bioprobe Applications. *Chem. - Eur. J.* **2010**, *16*, 12988–12994.

(26) Wang, H.; Wu, Y.; Yan, X. Room-Temperature Phosphorescent Discrimination of Catechol from Resorcinol and Hydroquinone Based on Sodium Tripolyphosphate Capped Mn-Doped ZnS Quantum Dots. *Anal. Chem.* **2013**, *85*, 1920–1925.

(27) Dan, L.; Wang, H. Mn-Doped ZnS Quantum Dot Imbedded Two-Fragment Imprinting Silica for Enhanced Room Temperature Phosphorescence Probing of Domoic Acid. *Anal. Chem.* **2013**, *85*, 4844–4848.

(28) Sang, L.; Wang, H. Aminophenylboronic-Acid-Conjugated Polyacrylic Acid–Mn-Doped ZnS Quantum Dot for Highly Sensitive Discrimination of Glycoproteins. *Anal. Chem.* **2014**, *86*, 5706–5712.

(29) Rohde, R. D.; Agnew, H. D.; Yeo, W. S.; Bailey, R. C.; Heath, J. R. A Non-Oxidative Approach toward Chemically and Electrochemically Functionalizing Si(111). *J. Am. Chem. Soc.* **2006**, *128*, 9518–9525.

(30) Wang, H.-F.; He, Y.; Ji, T.-R.; Yan, X.-P. Surface Molecular Imprinting on Mn-Doped ZnS Quantum Dots for Room-Temperature Phosphorescence Optosensing of Pentachlorophenol in Water. *Anal. Chem.* **2009**, *81*, 1615–1621.

(31) Bourlino, A. B.; Gournis, D.; Petridis, D.; Szabo, T.; Szeri, A.; Dekany, I. Graphite Oxide: Chemical Reduction to Graphite and Surface Modification with Primary Aliphatic Amines and Amino Acids. *Langmuir* **2003**, *19*, 6050–6055.

(32) Nonella, M.; Mathias, G.; Tavan, P. Infrared Spectrum of p-Benzoquinone in Water Obtained from a QM/MM Hybrid Molecular Dynamics Simulation. *J. Phys. Chem. A* **2003**, *107*, 8638–8647.

(33) Jutarosaga, T.; Jeoung, J. S.; Seraphin, S. Infrared Spectroscopy of Si–O Bonding in Low-dose Low-energy Separation by Implanted Oxygen Materials. *Thin Solid Films* **2005**, *476*, 303–311.

(34) Mendoza, M. F.; Hollabaugh, N. M.; Hettiarachchi, S. U.; McCarley, R. L. Human NAD(P)H:Quinone Oxidoreductase Type I (hNQO1) Activation of Quinone Propionic Acid Trigger Groups. *Biochemistry* **2012**, *51*, 8014–8026.

(35) Han, Y.; Shen, H.; Carr, B. I.; Wipf, P.; Lazo, J. S.; Pan, S. NAD(P)H:Quinone Oxidoreductase-1-Dependent and -Independent Cytotoxicity of Potent Quinone Cdc25 Phosphatase Inhibitors. *J. Pharmacol. Exp. Ther.* **2004**, *309*, 64–70.

(36) Hsieh, T.; Wu, J. M. Suppression of Cell Proliferation and Gene Expression by Combinatorial Synergy of EGCG, Resveratrol and γ -Tocotrienol in Estrogen Receptor-Positive MCF-7 Breast Cancer Cells. *Int. J. Oncol.* **2008**, *33*, 851–859.

(37) Bruge, F.; Virgili, S.; Cacciamani, T.; Principi, F.; Tiano, L.; Littarru, G. P. NAD(P)H:quinone Oxidoreductase (NQO1) Loss of Function in Burkitt's Lymphoma Cell Lines. *BioFactors* **2008**, *32*, 71–81.